Phys. Biol. **7** (2010) 046007 (14pp) doi:10.1088/1478-3975/7/4/046007

Collective cell motion in endothelial monolayers

A Szabó[1], R Ünnep[1], E Méhes[1], W O Twal[2], W S Argraves[2], Y Cao[3] and A Czirók[1,4,5]

[1] Department of Biological Physics, Eotvos University, Budapest, Hungary
[2] Department of Regenerative Medicine and Cell Biology, Medical University of South Carolina, Charleston, SC, USA
[3] Karolinska Institute, Stockholm, Sweden
[4] Department of Anatomy and Cell Biology, University of Kansas Medical Center, Kansas City, KS, USA

E-mail: andras@biol-phys.elte.hu

Received 10 September 2010
Accepted for publication 15 October 2010
Published 12 November 2010
Online at stacks.iop.org/PhysBio/7/046007

Abstract
Collective cell motility is an important aspect of several developmental and pathophysiological processes. Despite its importance, the mechanisms that allow cells to be both motile and adhere to one another are poorly understood. In this study we establish statistical properties of the random streaming behavior of endothelial monolayer cultures. To understand the reported empirical findings, we expand the widely used cellular Potts model to include active cell motility. For spontaneous directed motility we assume a positive feedback between cell displacements and cell polarity. The resulting model is studied with computer simulations and is shown to exhibit behavior compatible with experimental findings. In particular, in monolayer cultures both the speed and persistence of cell motion decreases, transient cell chains move together as groups and velocity correlations extend over several cell diameters. As active cell motility is ubiquitous both *in vitro* and *in vivo*, our model is expected to be a generally applicable representation of cellular behavior.

S Online supplementary data available from stacks.iop.org/PhysBio/7/046007/mmedia

1. Introduction

Cell motility is instrumental both in development and certain pathophysiologies [1, 2]. Collective motility of interacting cells is a poorly understood but fundamental aspect of these phenomena [3]. Such movements are required for important morphogenetic and pathological processes, for example, gastrulation, vasculogenesis, tumor growth, wound healing and revascularization of damaged tissues.

Arguably, cell sorting is the best studied process involving simultaneous displacement of closely packed cells [4, 5]. The differential adhesion hypothesis and its computational representations—based on the Potts model [6] or analogous lattice-free variants [7, 8]—successfully explain the outcome as well as the time course of cell sorting experiments. The cell types used in sorting experiments move diffusively within bulk uniform environments far from cell type boundaries [4], although some temporal and spatial correlations are detectable [5].

Less is known how polarized cells, which maintain their migratory direction in time, move in high-density cultures. Most studies addressing this problem have investigated the expansion of epithelial cell sheets or other monolayers into an empty area or 'wound'. During the expansion, cells at the monolayer boundary [9] or within a broader layer [10] exert substantial traction forces and are thought to pull the passive bulk of the sheet forward [4, 11].

Recent studies on the motion of kidney epithelial (MDCK [12]) or endothelial (HUVEC [13]) cells within monolayers, as well as immune cells in explanted lymph nodes [14], have indicated an intriguing motion pattern. These cells exhibit an apparently undirected, albeit correlated, streaming behavior even in the absence of directed expansion of the

[5] Author to whom any correspondence should be addressed.

holds asymptotically. Therefore, in figure 5(*c*) the asymptotic linear relation between the average cell displacement and neighbor separation with a slope of $\sqrt{2}$ indicates a substantial mixing and an uncorrelated long-term behavior within the monolayer.

Our statistical characterization thus revealed that endothelial monolayers move in locally anisotropic, 50–100 μm wide and 200–300 μm long streams, which form and disappear at random positions. In low density cell cultures cells in front of a moving cell tend to move in similar direction, but cell movements in lateral directions are uncorrelated. Despite the presence of streams, cell mixing is substantial in the monolayers: with a good approximation, movement of adjacent cells can be considered as independent persistent random walks.

3. Model definition

3.1. Cellular Potts model

To explain and model the emergence of collective flow patterns in cell monolayers, we adopted the two-dimensional cellular Potts model (CPM) approach. In theoretical studies the CPM is a frequently used method to represent the movement of closely packed cells [6, 14, 17–20]. The main advantage of the CPM approach is that cell shape is explicitly represented; thus, the simulation has the potential to describe dynamics in which controlled cell shape plays an important role [17, 21]. To obtain a biologically plausible, yet simple, model we consider below a positive feedback loop between cell polarity and cell movement in addition to the surface tension-like intercellular adhesion and cell compressibility. As we explain in detail below, the model assumptions are as follows.

(A1) Cells form a monolayer and each cell is simply connected.
(A2) Each cell has an approximately constant, pre-set size.
(A3) Cells adhere to their neighbors.
(A4) Each cell is capable of autonomous biased random motion. The direction bias (in a homogeneous environment) is set by an internal polarity vector.
(A5) The polarity vector has a finite lifetime, but it is reinforced by co-directional displacements of the cell.

In the CPM a non-negative integer value σ is assigned to each lattice site $\boldsymbol{x}$ of a two-dimensional grid. Two lattice sites are considered neighbors if they share a side (primary neighbors) or connect via a corner (secondary neighbors). Cells are represented as simply connected domains, i.e. a set of adjacent lattice sites sharing the same label σ. The label is equal to the cell index i ($0 < i \leqslant N$, where N is the number of cells in the simulation). Sites that belong to the irregularly shaped area devoid of cells are marked by the special value $\sigma = 0$.

Cell movement is the result of a series of elementary steps. Each step is an attempt to copy the spin value onto a random lattice site $\boldsymbol{b}$ from a randomly chosen adjacent site $\boldsymbol{a}$, where $\sigma(\boldsymbol{a}) \neq \sigma(\boldsymbol{b})$. This elementary step is executed with a probability $p(\boldsymbol{a} \to \boldsymbol{b})$. If the domains remain simply connected (A1), and thus cells do not break apart or form voids, the probability assignment rule ensures the maintenance of a target cell size (A2), adhesion of cells (A3) and active cell motion (A4, A5). For convenience and historical reasons p is given as

$$\ln p(\boldsymbol{a} \to \boldsymbol{b}) = \min[0, -\Delta u(\boldsymbol{a} \to \boldsymbol{b}) + w(\boldsymbol{a} \to \boldsymbol{b})], \quad (6)$$

where, as specified below in detail, w represents a bias responsible for the cell-specific active behavior considered, u represents a goal function to be minimized and $\Delta u(\boldsymbol{a} \to \boldsymbol{b})$ represents its change during the elementary step considered.

Since updating each lattice position takes more steps in a larger system, the elementary step cannot be chosen as the measure of time. The usual choice for the time unit is the Monte Carlo step (MCS), defined as L^2 elementary steps, where L is the linear system size [21].

3.2. Evaluating configurations

In the CPM approach, a goal function ('energy') is assigned [6] to each configuration. The goal function guides the cell behavior by distinguishing between favorable (low u) and unfavorable (high u) configurations as

$$u = \sum_{\langle \boldsymbol{x}, \boldsymbol{x}' \rangle} J_{\sigma(\boldsymbol{x}), \sigma(\boldsymbol{x}')} + \lambda \sum_{i=1}^{N} \delta A_i^2. \quad (7)$$

The first term in (7) enumerates cell boundary lengths. The summation goes over adjacent lattice sites. For a homogeneous cell population, the $J_{i,j}$ interaction matrix ($0 \leqslant i, j \leqslant N$) is given as

$$J_{i,j} = \begin{cases} 0 \text{ for } i = j \\ \alpha \text{ for } ij > 0 \text{ and } i \neq j \text{ (intercellular boundary)} \\ \beta \text{ for } ij = 0 \text{ and } i \neq j \text{ (free cell boundary).} \end{cases} \quad (8)$$

The surface energy-like parameters α and β characterize both intercellular adhesiveness and cell surface fluctuations in the model. The magnitude of these values determines the roughness of cell boundaries: small magnitudes allow dynamic, long and hence curvy boundaries, while large magnitudes restrict boundaries to straight lines and thus freeze the dynamics. In addition to cell boundary roughness, the parameters α and β also specify the preference of intercellular connections over free cell surfaces (A3). If two adhering cells are separated by inserting a layer of empty sites between them, then the change in u is proportional to $2\beta - \alpha$ at each site along the boundary line affected. Therefore, for $2\beta > \alpha$ free cell boundaries are penalized and the cells are adhesive [22].

The second term in expression (7) is responsible for maintaining a preferred cell area (A2). For each cell i, the deviation of its area from a pre-set value is denoted by δA_i. Parameter λ adjusts the tolerance for deviation. Thus, λ is related to the compressibility of cells in the 2D plane and also determines the magnitude of cell area fluctuations.

3.3. Cell polarity and active motility

While u evaluates configurations, w is assigned directly to the elementary steps and therefore allows the specification of a broader spectrum of cellular behavior [23]. Active cell motility involves cell polarity, a morphological, dynamical and biochemical difference between the cell's leading edge and tail

Table 2. Parameters used in the model.

Parameter name	Symbol	Value	Range	**Main, experimentally detectable effect(s)**
Cell–cell boundary cost	α	2	1–4	Cell boundary flexibility, cell shape
Free cell boundary cost (relevant only in single-cell simulations)	β	1	–	Cell boundary flexibility, cell shape, surface tension of aggregates.
Target cell area	A	50	–	Cell–cell distance
Area constraint coefficient	λ	1	0.5–2	Cell size fluctuations
Self-propulsion coefficient	P	2	0.5–4	Average cell speed
Decay rate of cell polarity	r	0.2	0.8–0.02	Persistence time of cell motion

[24, 25]. In this study we model active cell motility by first assigning a cell polarity vector $\boldsymbol{p}_k$ to each cell k (A4). We then increase the probability of those elementary conversion steps that advance the cell center in the direction parallel to $\boldsymbol{p}_k$, as

$$w(\boldsymbol{a} \to \boldsymbol{b}) = P \sum_{k=\sigma(a),\sigma(b)} \frac{\Delta \boldsymbol{X}_k(\boldsymbol{a} \to \boldsymbol{b})\boldsymbol{p}_k}{|\boldsymbol{p}_k|}. \tag{9}$$

Parameter P sets the magnitude of the bias and $\Delta \boldsymbol{X}_k$ represents the displacement of the center of cell k during the elementary step considered.

The cell polarity vector is an attempt to represent the localization and magnitude of the biochemical changes characterizing the leading edge of a migratory cell. It is not yet clear what is the molecular polarization mechanism in endothelial cells. The best documented front/rear polarization mechanisms involve either the mutual inhibition of Rac and Rho, key GTPase 'switches' of cell motility [1, 26] and/or the accumulation of the phosphatidylinositol membrane component PIP_3 [27, 28]. The accumulation of active Rac1 (and PIP_3) at the leading edge is thought to activate a biochemical cascade that involves the Arp2/3 complex providing new actin nucleation sites. The Rac1-Arp2/3 cascade eventually results in a local increase in actin polymerization, pushing the plasma membrane forward [1, 27]. Through positive feedback loops, both the Rac/Rho and PIP_2/PIP_3 systems are thought to be able to amplify slight spatial differences in upstream inputs and even develop a spontaneous polarity [27, 28]. This amplification of presumably random receptor activity and the related spontaneous symmetry breaking could explain the onset of spontaneous cell motility in a homogeneous environment and motivates the use of a unit vector in rule (9).

Even less molecular details are known about what drives changes in cell polarity in the absence of external cues such as chemoattractant gradients. However, in a motile cell the polarization direction must change eventually. For instance, when the advance of the leading process is impaired and the process collapses, a new migration direction is selected and cell polarity is altered. We propose to update the cell polarity vectors by considering a spontaneous decay and a reinforcement from cell displacements (A5). In each MCS the change in $\boldsymbol{p}_k$ is

$$\Delta \boldsymbol{p}_k = -r\boldsymbol{p}_k + \Delta \boldsymbol{X}_k, \tag{10}$$

where r is the rate of spontaneous decay and $\Delta \boldsymbol{X}_k$ is the displacement of the center of cell k during the MCS considered. A characteristic memory length T of the polarization vector is defined as $T = 1/r$.

Rules (9) and (10) together constitute a positive feedback loop. In this model, steric constraints may result in co-migration of adjacent cells as the retraction of one cell allows for the expansion of the other. The resulting expansion of cell bodies (like the actin polymerization process in real cells) can therefore alter and synchronize cell polarity. The molecular mechanism for cell polarity reinforcement by cell motility may involve either the stabilization of PIP_3 accumulation by actin polymerization [29–31] or the activation of Rac1 by microtubule dynamics [32, 33].

4. Simulation results

We have chosen the open source tissue simulation toolkit [21, 34] as our CPM framework, in which we implemented our extensions as C++ codes. We refrain from using a temperature-like parameter, as rule (3) of [6], analogous to our rule (6), simply scales each CPM parameter α, β and λ by the temperature, a constant. Thus, when comparing our studies with those that include a temperature in the simulations, our parameter values are to be compared with the corresponding values divided by the temperature.

Model simulations with $N = 1000$ cells were performed in a 200×200 lattice, with parameters $\alpha = 2$, $\lambda = 1$ and $P = 2$, T = 5 MCS (see table 2 for a summary of the parameter values used). After scaling by temperature, our parameters are within the same range as those in previous studies [6, 20, 21, 35]. We applied closed boundary conditions (immutable empty sites at the border) in the simulations.

The spatial scale of the model is easily determined by comparing the empirical and simulated cell sizes. The target cell area was set to 50 lattice sites, yielding a distance of about 7 sites between cell centers in the monolayer. This compares to the experimentally observed 35 μm, calibrating a distance of one lattice site to 5 μm. The duration of a MCS is calibrated by comparing empirical and simulated cell speeds (see below) resulting in one MCS to correspond to 1 min, a value similar to the ones used in other CPM studies [20, 21].

4.1. Individual cells perform a persistent random walk

Model simulations of single cells were performed with Potts parameters $\beta = 1$ and $\lambda = 1$ (the parameter α is irrelevant under these conditions). Figure 6(*a*) reveals that in the absence of active motility ($P = 0$) the average displacement $d(t)$ grows with time t as

$$d(t, P = 0) \sim \sqrt{t}. \tag{11}$$

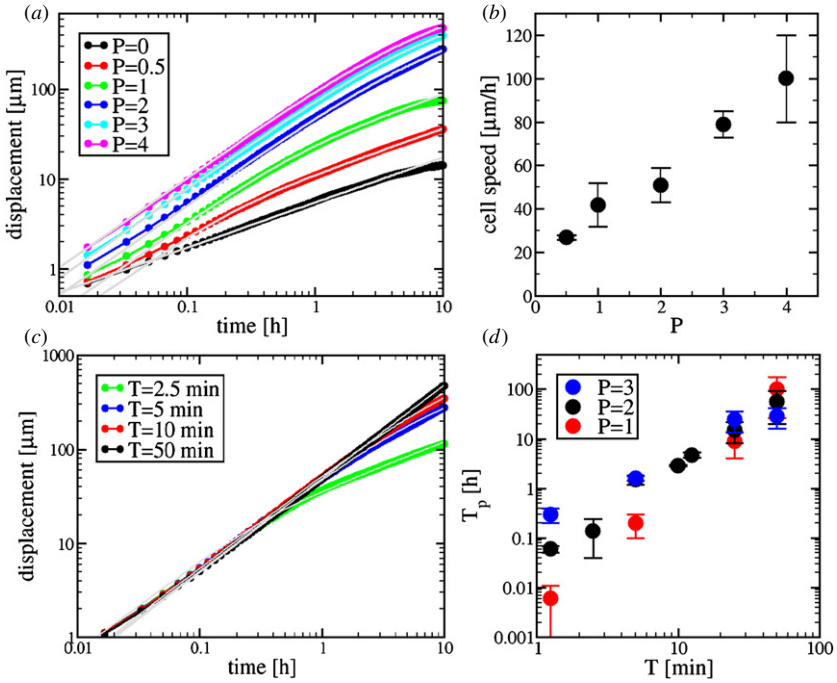

Figure 6. Motion statistics of individual, non-interacting cells in model simulations. (*a*) Average displacement $d(t)$ versus time t. Values of P are shown in the key, $\beta = 1$, $\lambda = 1$, $T = 5$ min. Gray solid lines are fits by the persistent random walk formula (2) and a square-root function in the case of $P = 0$. (*b*) The speed S of directed motion is set by the parameter P. (*c*) Average displacement versus time curves and the corresponding fits, obtained from simulations with various polarization memory lengths. Values of T are shown in the key, $\beta = 1$, $\lambda = 1$, $P = 2$. (*d*) The persistence time of the random walk behavior, T_p, mostly depends on T through a nonlinear relation, and to a lesser extent also on the active motion parameter P.

Thus, as in the original CPM [4, 5], cell movement is diffusive for $P = 0$. Large values of P result in unrealistic cell shapes and behavior as the effects of the other constraining terms in expression (7) diminish. The active motility rules (9) and (10) with $0 < P < 4$ result in individual cells performing a persistent random walk: as figures 6(*a*) and (*c*) demonstrate, the average displacements are well fitted by equation (2) for $d(t, P) > 1$.

As figure 6(*b*) reveals, the speed of active motion S is proportional to P in the $0 < P < 4$ range (the parameter P is bounded by the connectivity constrains of the model). Because of the positive feedback between directed cell motion and maintenance of cell polarity in our model, the persistence time T_p increases strongly both with P and the duration of the memory T (figure 6(*d*)).

4.2. Streaming behavior in monolayer simulations

Monolayer simulations result in behavior similar to the experimentally observed streaming motion, with shear lines and vortices present (figure 7(*a*) and movie 2 (available at stacks.iop.org/PhysBio/7/046007)). Motion within the monolayer is somewhat hindered when compared with individual cells, as the speed and persistence time decrease by 20% (figure 7(*b*)). In addition to qualitative similarity, the calculation of flow fields allows for a more rigorous comparison of model simulations to empirical data (figure 8, to be compared with figures 3 and 4). Lateral correlations and back-flow are reduced when non-adherent cells are simulated at lower cell densities (figure 8(*b*)). At subconfluent densities the average flow field still reveals the 'steric' repulsion of cells in the path of an actively moving cell.

4.3. Parameters

We introduced two new parameters, P and T, in addition to the usual CPM parameters describing free and intercellular boundaries (α and β) and compressibility λ. In monolayer simulations there are no free cell boundaries; therefore, the parameter β is irrelevant. Parameter sensitivity analysis revealed that the model can also exhibit an ordered phase. In this phase, responding to the closed boundary conditions, all cells participate in a single, system-wide rotational movement. This state is reached by increasing the memory duration T. For increasing T (but still below the threshold needed for the formation of a single vortex), the streams become wider (figure 9(*a*) and movie 3 (available at stacks.iop.org/PhysBio/7/046007)). Conversely, by decreasing either T or P, a diffusive state is recovered, where the persistence length is smaller than the size of a cell (movie 4 available at stacks.iop.org/PhysBio/7/046007). In this limit $\boldsymbol{V}(\boldsymbol{x})$ is well approximated by the flow field of an incompressible fluid around a moving disk: V_x decays as x^{-2} and $-y^{-2}$ along the x and y axes, respectively. Increasing P or T results in wider and longer streams (figure 9(*e*)–(*h*)).

The d_2 separation of adjacent cell pairs, when plotted against the mean cell displacement d (figure 9(*b*) and (*d*)), reveals the system-wide ordered flow, when cells can cover

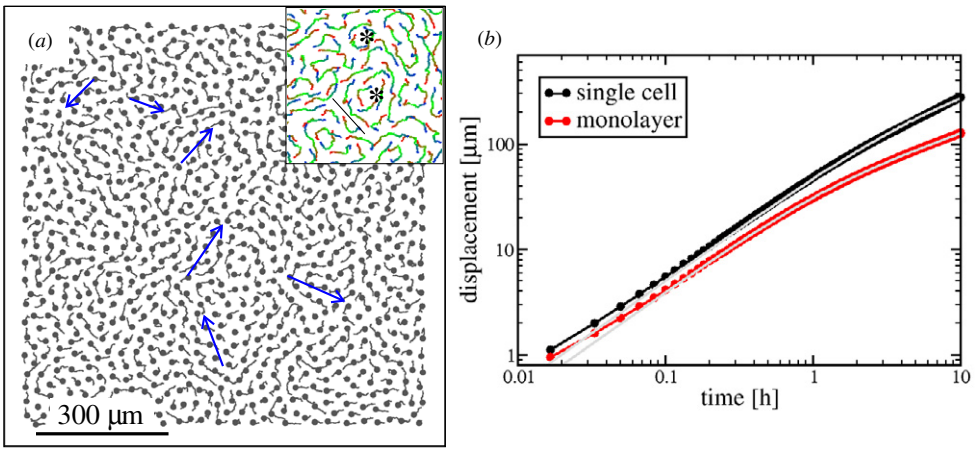

Figure 7. Motion characteristics in monolayer simulations. A representative parameter setting was chosen as $P = 2$, $T = 5$ min, $\alpha = 2$, $\beta = 1$ and $\lambda = 1$. (*a*) Model cell trajectories, from a 40 min long time interval, reveal streams formed by several cells (blue arrows). The inset shows trajectories from a 90 min long interval, color-coded progressively from older to newer as red to green to blue. A shear line separating streams moving in opposite directions (black line) and two vortices (asterisks) are indicated. (*b*) Average displacements of single, unconstrained cells are greater than those in a monolayer. Persistence time and cell speed in a monolayer fall from 40 to 30 min and from 55 μm h^{-1} to 40 μm h^{-1}, respectively.

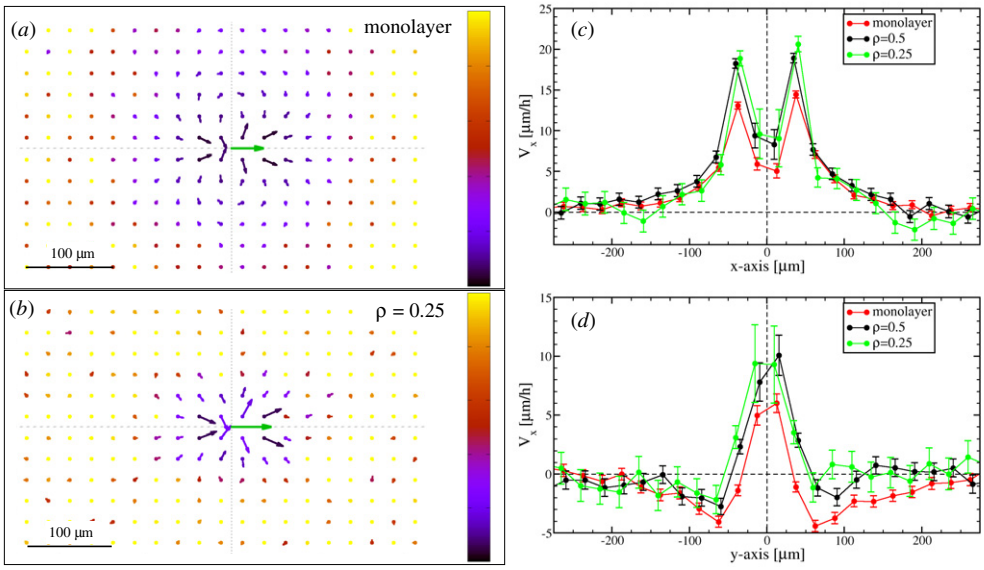

Figure 8. Flow fields $\boldsymbol{V}(\boldsymbol{x})$ around a moving cell within a monolayer (*a*) and a subconfluent culture (*b*) simulation. The corresponding parallel and perpendicular velocity profiles are shown in panels (*c*) and (*d*), respectively. Cell density values specified in the keys are normalized to confluent culture density ($\rho = 1$). In low density cultures correlations are reduced in the lateral direction. Velocity vectors represent 1 h displacements; the green arrow indicates the average velocity of the cells. As in figure 3, the color code in panels (*a*) and (*b*) indicates the estimated relative SEM, and the color scale represents the interval [0 : 1].

large displacements without changing their neighbors ($d \gg d_2/\sqrt{2}$). In the streaming regime the asymptotic relation (5) holds indicating uncorrelated motion within the monolayer.

Depending on the values of P and T, increasing α can result in a multitude of changes. Reflecting its definition, a simulation with higher α values yields cells with smoother boundaries (figures 10(*b*) and (*d*)). In general, reducing the freedom of cell boundary movement hinders cell intercalation, and thus movement within a monolayer. This is indicated by decreasing speeds with increasing α (data not shown). However, if self-propulsion is strong enough, the reduced intercalation can also yield wider streams as demonstrated by figures 10(*c*), (*e*) and (*f*).

Our model for actively moving cells in a monolayer culture is thus capable of explaining most experimental observations presented in section 2. Furthermore, the simple model structure allows a thorough mapping of the parameter space. We find it remarkable that a given pair of (P, T) parameters yield individual cell speeds, persistence times in the correct range as well as a collective behavior comparable with the observed streaming. In particular, $T = 5$ min is a plausible value for the time needed to alter cell polarity.

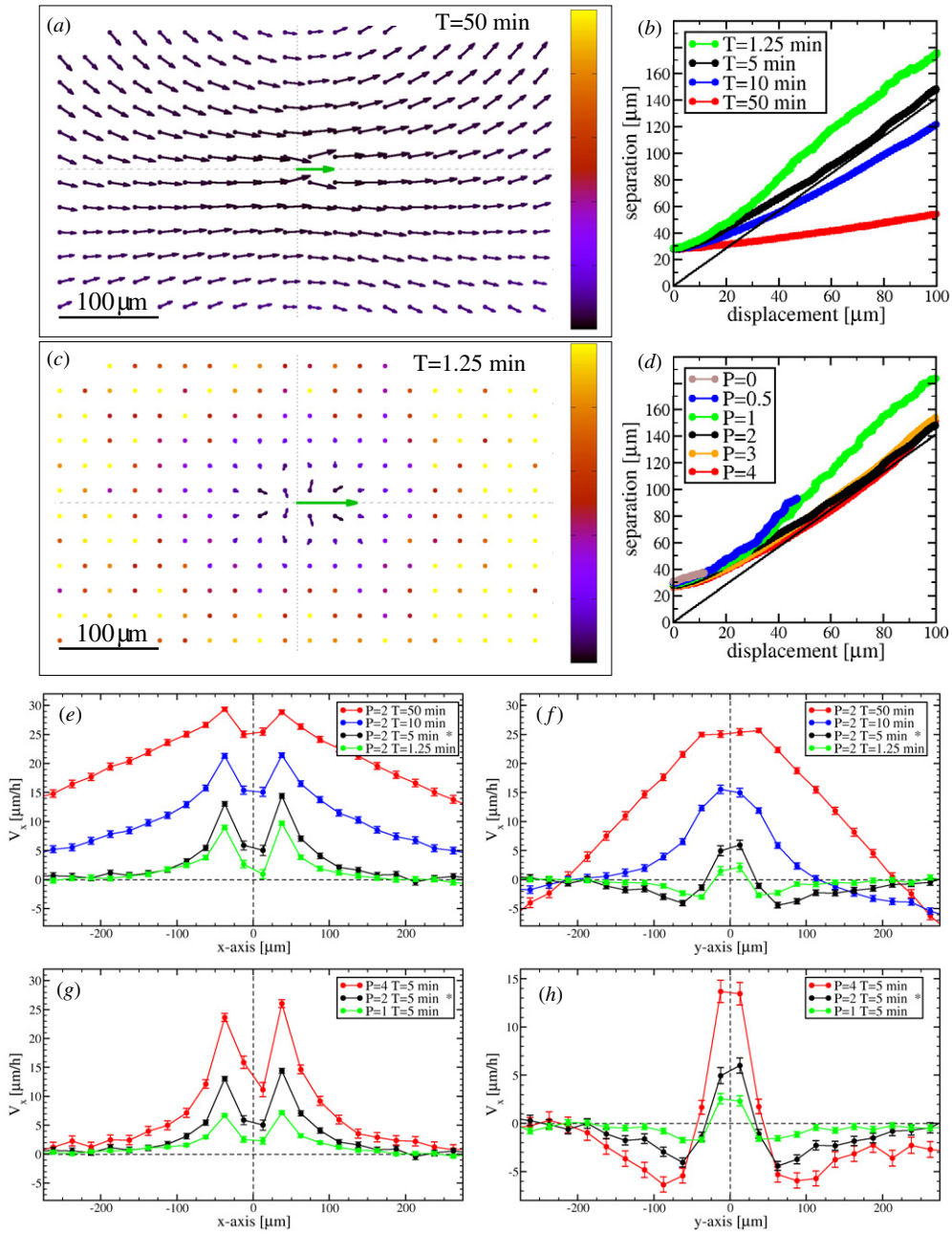

Figure 9. The self propulsion parameters, P and T, play a crucial role in defining the collective behavior of the monolayer. Flow fields $\boldsymbol{V}(\boldsymbol{x})$ are shown for long ((*a*) $T = 50$ min) and short ((*c*) $T = 1.25$ min) memory duration of cell polarity. The remaining parameters are the same as in figure 7. Flow fields are presented as in figure 8. The corresponding parallel and perpendicular velocity profiles are shown in panels (*e*) and (*f*), respectively. Increasing T results in wider, longer and faster streams. Similar but less dramatic tendencies are seen when changing P (panels (*g*) and (*h*)). For large enough T, the system organizes into a phase where the correlation length is comparable to the system size. Movement within the monolayer is diffusive in the streaming regime as the average neighbor separation versus cell displacement curves (panels (*b*) and (*d*)) are consistent with the asymptotic behavior of equation (5), shown as the solid line. In the globally ordered (rotating) regime cells move further without separating. The asterisk marks the parameter values used in figure 7.

With this value, it is possible to obtain cell speeds in the range of 20–40 μm h^{-1} within monolayers and 50 μm h^{-1} for individual cells. Our empirical data show cell speeds between 10 and 30 μm h^{-1} for monolayers. A similarly close and independent agreement is obtained for the persistence times, at approximately 1 h both in the model and in the experiments. The spatial structure of streams is strongly anisotropic, being approximately 200–300 μm long and 100 μm wide in both the experiments and in the simulations.

5. Discussion

While correlated cell velocities and streams in MDCK and HUVEC monolayers were recently reported [12, 13], their

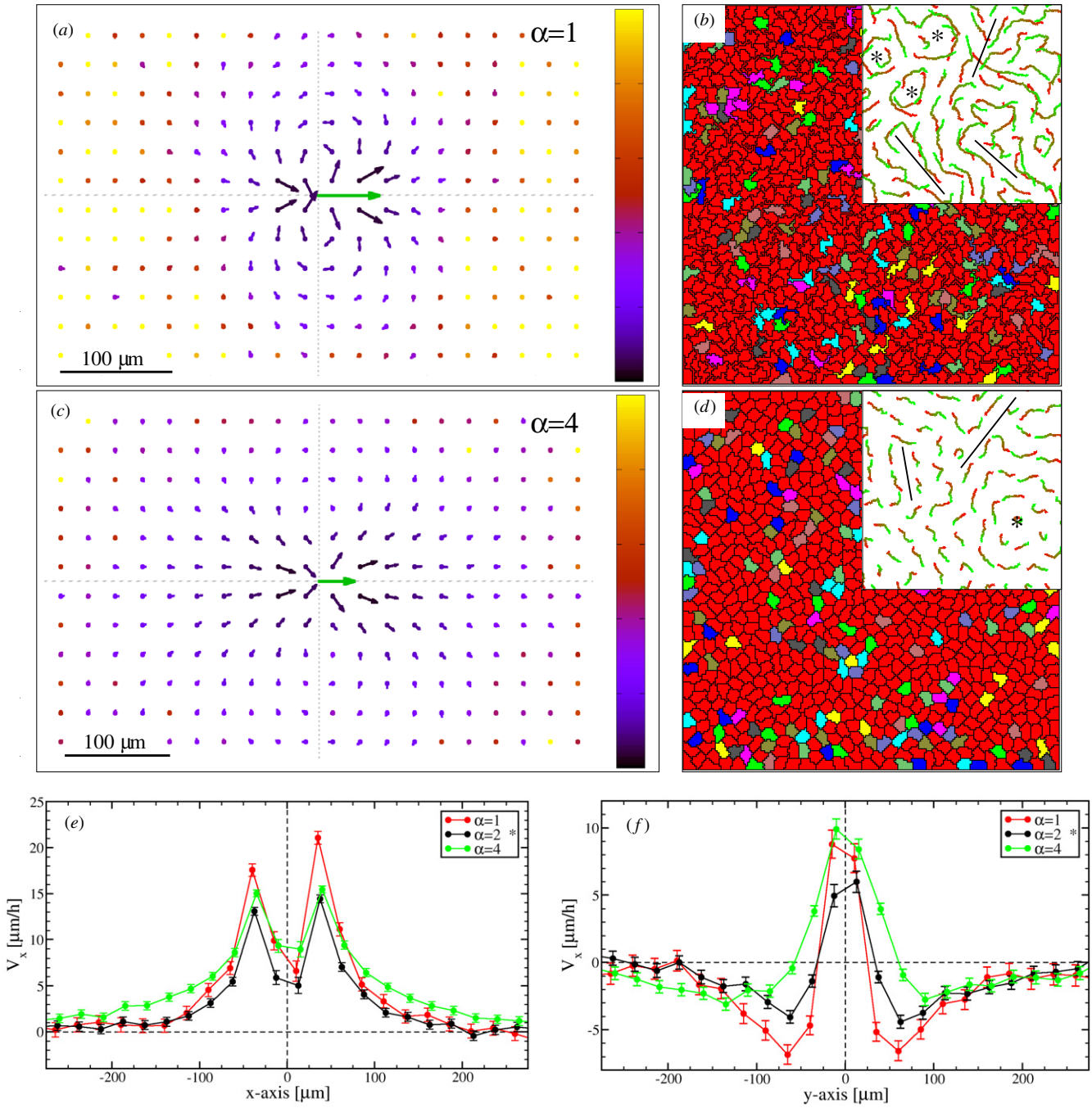

Figure 10. Role of cell adhesion parameter α. Simulation results are compared for $\alpha = 1$ (panels (*a*), (*b*)) and $\alpha = 4$ (panels (*c*), (*d*)). Self-propulsion is strong ($P = 3$), while the remaining parameters are the same as in figure 7. As the configurations demonstrate (panels (*b*), (*d*)), parameter α controls the cell shape and cell boundary smoothness. The $\boldsymbol{V}(\boldsymbol{x})$ flow fields (panels (*a*), (*c*)) and their profiles along the parallel (*e*) and perpendicular (*f*) axes reveal that the streams get wider with increasing α as cells cannot easily intercalate. Flow fields are presented as in figure 8. The insets in panels (*b*) and (*d*) demonstrate cell trajectories, comparable with similar plots in figures 1 and 7. The asterisk marks the parameter values used in figure 7.

dynamics remained largely unexplained. To obtain further empirical data to test our model, we systematically investigated monolayer cultures of three different endothelial cell lines. Our finding that 5–20 cells move together in narrow, chain-like groups is in accord with previous reports. Because our cultures were grown in a monolayer, our measured cell speeds and persistence times ($S \approx 10 - 30\ \mu\mathrm{m\,h^{-1}}$, $T \approx 1$ h) somewhat differ from the values previously reported for individual endothelial cells ($S \approx 40\ \mu\mathrm{m\,h^{-1}}$, $T \approx 3$ h [36]; $S \approx 50\ \mu\mathrm{m\,h^{-1}}$, $T \approx 0.6$ h [37]).

5.1. Models for collective cell movements

Previous theoretical studies on cell movement include a multi-particle model that was proposed to explain the collective